Iron catalysts supported on carbon nanotubes for Fischer–Tropsch synthesis: effect of pore size

R. M. Malek Abbaslou, J. Soltan, S. Sigurdson & A. K. Dalai
Catalysis & Chemical Reaction Engineering Laboratories, Department of Chemical Engineering, University of Saskatchewan, Saskatoon, Canada

Abstract

In this report, the effects of pore diameter and structure of iron catalysts supported on carbon nanotubes (CNTs) on Fischer–Tropsch (FT) reaction rates and product selectivities are presented. Two types of CNTs with different average pore sizes (12 and 63 nm) were prepared. The CNTs were chosen in a way to have comparable surface areas so as to eliminate the effects of different surface areas. The iron catalysts (the narrow pore catalyst denoted Fe/np-CNT and wide pore catalyst denoted Fe/wp-CNT) were prepared using incipient wetness impregnation method and characterized by ICP, BET, XRD, TPR, SEM and TEM analyses. The TEM and XRD analysis showed that the iron oxide particles on the Fe/wp-CNT (17 nm) were larger than those on Fe/np-CNT sample (11 nm). TPR analyses of the catalysts showed that the degree of reduction of the Fe/np-CNT catalyst was 17% higher compared to that of the Fe/wp-CNT catalyst. For the FT reactions, it was found that the activity of the np-CNT catalyst (%CO conversion of 31) was much higher than that of the wp-CNT catalyst (%CO conversion of 11). Also, the Fe/wp-CNT was more selective toward lighter hydrocarbons with a methane selectivity of 41% whereas, the methane selectivity of the np-CNT catalyst was 14%. It can be concluded that the deposition of the metal particles on the CNT with narrow pore size (in the range of larger than 10 nm) results in more active and selective catalyst due to higher degree of reduction and higher metal dispersion.

Keywords: Fischer–Tropsch synthesis, iron, carbon nanotubes, pore size.

WIT Transactions on Ecology and the Environment, Vol 121, © 2009 WIT Press
www.witpress.com, ISSN 1743-3541 (on-line)
doi:10.2495/ESU090141

1 Introduction

Fischer–Tropsch (FT) synthesis is a potentially attractive technology for production of clean liquid fuels from syngas. The syngas can be supplied through gasification of coal or biomass and reforming of natural gas. FT synthesis proceeds on metal (Fe, Co and Ru) supported catalysts. The efficiency of the FT synthesis can be enhanced by design of new catalysts with higher syngas conversion, higher C_5+ yield, and lower methane selectivity [1–2]. In the FT processes, the catalyst activity and selectivity are influenced by nature and structure of the support, nature of the active metal, catalyst dispersion, metal loading, and catalyst preparation method [3]. Most studies on FT catalysts have been carried out with the metals supported on silica, alumina or titania and their structural properties such as pore size have been studied [4]. Recently, carbon nanotubes (CNTs) as a new support have been investigated for FT reactions [5–11].

Carbon nanotubes with unique properties such as uniform pore size distribution, meso and macro pore structure, inert surface properties, and resistance to acid and base environment can play an important role in a large number of catalytic reactions [11]. CNTs are different than the other supports in that they have graphite layers with a tubular morphology [7–8]. Also, CNT structure such as inner and outer diameter and length of nanotubes can be manipulated using different synthesis processes and operating conditions. Literature review including our previous work on the application of CNTs as support for catalytic reactions especially FT reactions have shown that CNTs can be considered an alternative support which can improve performance of metal catalyst compared to the other supports [4–9,12]. However, the effects of pore size and diameter of carbon nanotubes on the catalytic performance of FT catalysts have not comprehensively been studied. In general, pore size of supported catalysts can influence particle size distribution, dispersion, extent of reduction, and mass transfer rates [4].

In this report, the effects of pore diameter of the support CNTs on FT reaction rates and selectivities over iron catalysts are presented. Two types of CNTs with different average pore sizes (10 and 63 nm) were prepared in a way to have comparable surface areas so as to remove the effects of different surface areas.

2 Experimental

In order to analysis solely the effects of inner pore of CNTs on the performance of the iron catalyst for the FT reactions, two CNT samples with considerable difference in the pore diameters were used. The narrow pore CNT sample (denoted as np-CNT) was purchased. The wide pore CNT sample (denoted as wp-CNT) was synthesized using anodic aluminum oxide (AAO) films and chemical vapor deposition method. The details of synthesis procedure were given in our previous paper [12].

Both CNT samples were treated in nitric acid (60 wt%) at 110^{o}C for 16 hours. The catalysts were prepared according to the incipient wetness impregnation

method. For the preparation of the catalyst with iron particles inside the nanotube pores with 20 wt% Fe, an appropriate amount of $Fe(NO_3)_3 \cdot 9H_2O$ was dissolved in deionised water. The volume of the salt solution was equal to total pore volume of the CNT samples. In this case, the metal solution filled the inner pores of the CNTs due to capillary effects [5]. After drying at 120°C and calcination at 400°C for 3 hours, the catalysts were characterized by nitrogen adsorption, ICP, TPR, XRD, SEM and TEM.

The surface area, pore volume of the CNTs and catalysts were measured by an ASAP-2000 Micromeritics system. The samples were degassed at 200°C for 2 h under 50 mTorr vacuum and their BET surface area and pore volume were determined.

XRD analysis was performed using a Philips PW1840 X-ray diffractometer with monochromatized Cu/Kα radiation. The crystallite diameter was estimated using Debye–Scherrer equation

The reduction behavior of the catalyst precursors was studied by temperature programmed reduction (TPR) using a CHEMBET-3000 equipped with a thermal conductivity detector. 0.1 g of the catalyst was placed in U-shaped quartz tube. A 5% hydrogen/nitrogen mixture was introduced (flow rate = 36 cm^3 (STP)/min) and the furnace was ramped from room temperature to 1173K at 10 K/min.

Morphology of the samples was studied by transmission electron microscopy (TEM). Sample specimens for TEM studies were prepared by ultrasonic dispersion of the catalysts in ethanol, and the suspensions were dropped onto a copper grid. TEM investigations were carried out using a Hitachi H-7500 (120kV). Several TEM micrographs were recorded for each sample and analyzed to determine the particle size distribution. A Phillips SEM-505 scanning electron microscope operating at 300 kV in SE display mode was also used. For characterization prior to analysis, all the samples were gold coated in a sputter coating unit (Edwards Vacuum Components Ltd., Sussex, England).

The Fischer–Tropsch synthesis was performed in a fixed-bed micro reactor. Prior to CO hydrogenation, in-situ reduction was conducted according to the following procedure. The catalyst (0.5 g) was placed in the reactor and diluted with 5 g silicon carbide. Then pure hydrogen flow was established at a rate of 45 ml/min. The reactor temperature was increased from room temperature to 380°C at a rate of 1°C/min and maintained at this activation condition for 14 h. After the activation period, the reactor temperature was decreased to 275°C under flowing hydrogen. Hydrogen and syngas flow rates were controlled by Brooks 5850 mass flow controllers. Argon was used as internal standard gas in the reactor feed. The mixed gases (30%CO, 60%H2, 10% Ar) entered the top of the fixed bed reactor. The temperature of the reactor was controlled via a PID temperature controller. Synthesis gas with a space velocity of 7200 cm^3(STP)/(h g) was introduced and the reactor pressure was increased to 2 MPa. Products were continuously removed from the vapor and passed through two traps. The pressure of uncondensed vapor stream was reduced to atmospheric pressure. The composition of the outlet gas stream was determined using an on-line GC-2014 Shimadzu gas chromatograph. The contents of traps were removed every 24 h, the hydrocarbon and water fractions were separated, and then analyzed by Varian

3400 GC. Catalytic activity and product selectivity were calculated after a time on stream of 50 hours.

3 Results and discussions

3.1 Supports and catalysts characterizations

SEM images (Figure 1a and 1b) of the acid-treated and purified CNTs samples (np-CNT and wp-CNT) revealed that the samples contained solely CNTs and no other impurities such as amorphous carbon was observed. Figure 1a shows that the np-CNT sample contained woven nanotubes with high aspect ratios. For wp-CNT sample, SEM image (Figure 1b) exhibited that nanotubes were well-aligned and the caps of nanotubes were open.

TEM images of the acid-treated CNT samples are given in Figure 2a and 2b. Figure 2a shows that the np-CNT sample had uniform nanotubes diameter and their inner and outer diameters varied between 8-12 nm and 20-25 nm, respectively. TEM analysis also revealed that a vast majority (more than 70%) of the np-CNT sample possessed open caps nanotubes (Fig 2a). As seen in Figure 2b, the wp-CNT sample comprised of straight nanotubes with diameter of 50-70 nm along with several Y junctions with inner diameters of 30-50 nm. The thickness of the walls varied in 7-9 nm range.

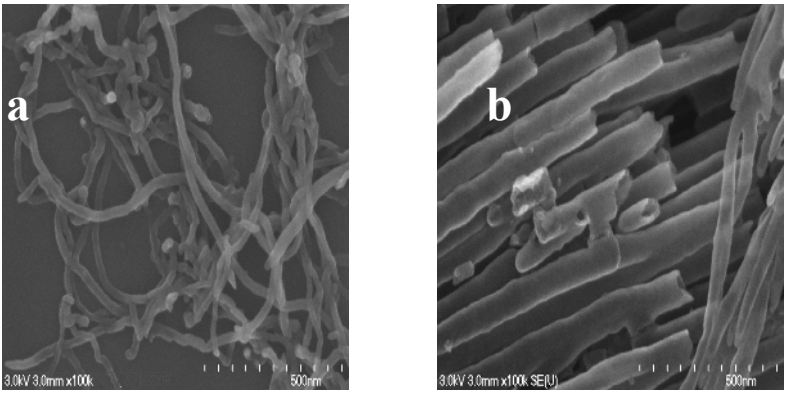

Figure 1: SEM micrograph of the CNT supports, a) np-CNT, b) wp-CNT.

The particle size distribution and position of the iron particles inside or outside of the CNTs were studied using several TEM images from each of the catalyst samples. Figure 3a and 3b show a representative TEM image of the iron catalyst supported on narrow pore CNT sample (Fe/np-CNT) and iron catalyst supported on wide pore CNT sample (Fe/wp-CNT). Dark spots represent the iron oxides which are attached inside or outside of the nanotubes. For both catalysts, a vast majority of the iron particles (80%) were distributed in the inner pores of CNTs (Fig. 3a and 3b). This can be attributed to carbon nanotubes' tubular structure which can induce capillary forces during the impregnation process. In

the case of Fe/np-CNT, the size of iron oxide particles varied from 4 to 14 nm with most abundant particles with a diameter of 8-10 nm. Whereas in the case of Fe/wp-CNT catalyst, particle size covers a wide range varying form 5 to 65 nm with the most abundant particle size of 14-21 nm. The data suggest that inner pore of nanotubes physically restricted the particle size growth unless the particle was located on the exterior surface of the nanotubes.

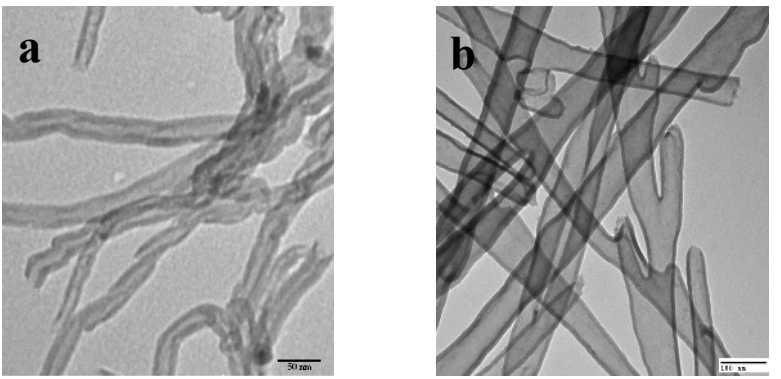

Figure 2: TEM images of CNT supports a) np-CNT b) wp-CNT.

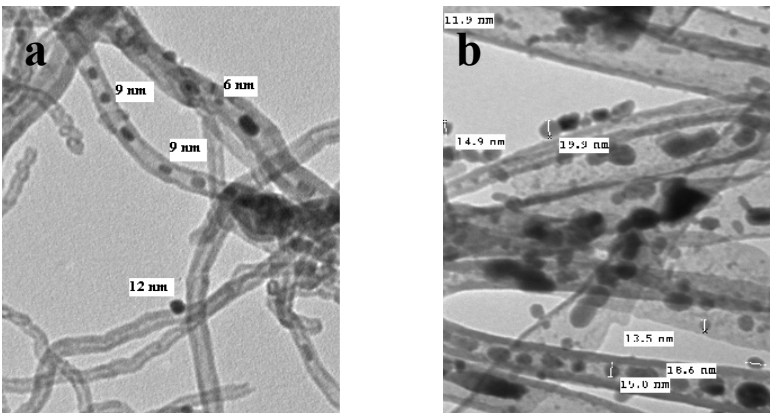

Figure 3: TEM images of the iron catalysts a) Fe/np-CNT b) Fe/wp-CNT. Dark spots represent the iron oxide particles inside and outside of the nanotubes.

Table 1 shows the metal content for the Fe/np-CNT and Fe/wp-CNT catalysts. ICP analyses of the catalysts revealed that the metal contents of the catalysts were fairly similar and close (±0.4%) to the target metal content of 20 wt% Fe. Table 1 also shows the results of surface area measurements of both CNT supports and corresponding iron catalyst. As discussed earlier, both CNT samples had a comparable surface areas (212 m^2/g for np-CNT and 218 m^2/g for

wp-CNT). As a result, both Fe/np-CNT and Fe/wp-CNT catalysts held similar metal loading per surface area of the supports. According to the N_2 adsorption analysis, the loading of 20% Fe decreased the surface area of Fe/np-CNT and Fe/np-CNT catalysts to 155 and 186 m_2/g, respectively. These data show that the BET surface area of the catalysts were lower than that of the supports indicating pore blockage due to iron loading on the supports. However, comparison between BET surface area of the Fe/np-CNT and Fe/wp-CNT catalysts showed that the extent of pore blockage in the Fe/np-CNT was higher than that in Fe/wp-CNT.

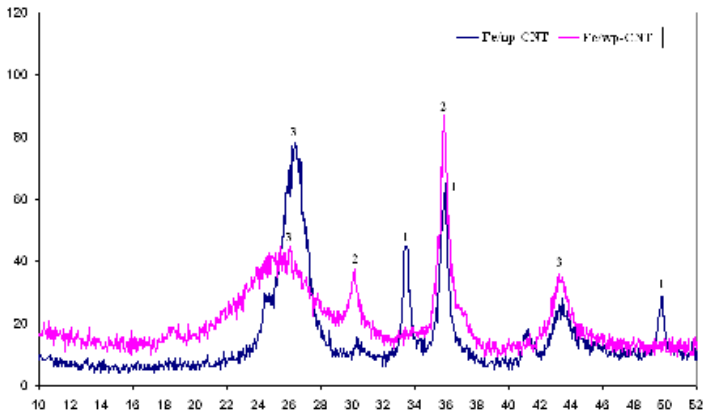

Figure 4: XRD spectra of Fe/np-CNT and Fe/wp-CNT. (1: Fe_2O_3, 2:Fe_3O_4, 3: CNT).

Table 1: Metal content and surface properties of CNT samples, Fe/np-CNT and Fe/wp-CNT catalysts.

Catalyst Name	Metal Content%[1]	BET Surface Area (m^2/g)	Total Pore Volume (cm^3/g)
np-CNT-support	0	212	0.58
wp-CNT-support	0	218	0.55
np-Fe/CNT	19.6	155	0.44
wp-Fe/CNT	20.1	186	0.48

1-Determined by ICP analysis.

Figure 4 shows XRD patterns of the calcined Fe/np-CNT and Fe/np-CNT catalysts. For both catalysts, the peaks at about 26 and 44° correspond to the graphite layers of multi-walled nanotubes. Surprisingly, the Fe/np-CNT and Fe/wp-CNT catalyst did not show similar XRD patterns. According to the XRD spectra, the diffraction peaks for Fe/np-CNT catalyst matched very well with the standard Hematite (Fe_2O_3) phase. Whereas, for Fe/wp-CNT catalysts, the peaks at 2θ of 30 and 35.7° exhibited the standard Magnetite (Fe_3O_4) phase.

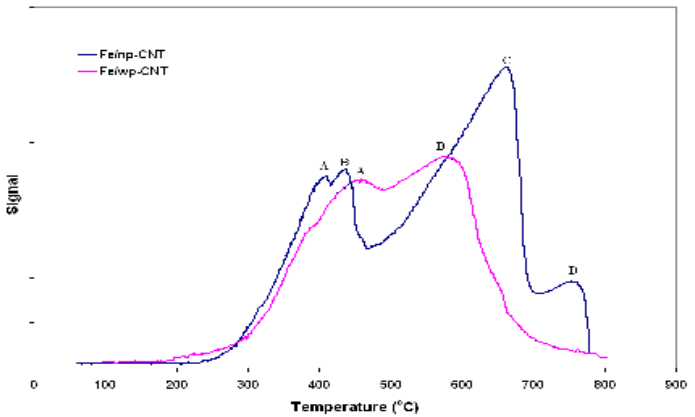

Figure 5: H_2-TPR profiles for Fe/np-CNT and Fe/np-CNT catalysts.

Table 2 shows the average iron oxides particle sizes on the catalysts calculated from XRD spectrum using Debye–Scherrer equation at the most intense peak of 36°. The data verified that the iron oxide on Fe/wp-CNT (17 nm) grew larger than that of on the Fe/np-CNT catalysts (11nm). To compare the particle size calculated based on XRD with TEM analysis, the size distribution of the particles is also shown in Table 2. There is a good agreement between the data for average particle size calculated based on XRD and the most abundant sizes from TEM analysis.

TPR analyses were performed to evaluate the reducibility of the Fe/np-CNT and Fe/wp-CNT catalysts . TPR patterns of Fe/np-CNT and Fe/np-CNT catalysts are shown in Figure 5. Four peaks (A, B, C and D) can be observed on the TPR profile of the Fe/np-CNT catalyst. Whereas, two peaks appeared on the TPR profile of the Fe/wp-CNT catalysts. Generally, the reduction of iron oxides takes place as below [10]:

$$Fe_2O_3 \rightarrow Fe_3O_4 \rightarrow FeO \rightarrow Fe$$

In the case of Fe/np-CNT, the first peak (A) can be assigned to the reduction of Fe_2O_3 to Fe_3O_4. The second peak, B, can be assigned to the subsequent reduction of Fe_3O_4 to FeO. Peak C, observed at 500-700 °C, can be related to the reduction of FeO to metallic Fe. Peak D can be attributed to gasification of CNTs at a temperature higher than 600°C. For Fe/wp-CNT catalyst, since the iron oxide was in the form of Fe_3O_4, the first peak (A) corresponded to the reduction

Table 2: Particle sizes (iron oxide) based on XRD and TEM analysis.

Catalyst	$d_{(Fe2O3)}$ [a] nm	$d_{(Fe2O3)}$ [b] nm
Fe/np-CNT	11	8-10
Fe/wp-CNT	17	14-21

a) Based on XRD analysis.
b) Based on TEM analysis.

Table 3: Reduction temperature (°C) and extent of reduction (from 25-800°C) based on H_2-TPR analysis.

Catalyst	Peak A	Peak B	Peak C	Peak D	Extent of reduction (25-700°C)
Fe/np-CNT	401	438	667	747	69
Fe/wp-CNT	459	574	-	-	52

of Fe_3O_4 to FeO and the second peak, B, can be assigned to the subsequent reduction of FeO to Fe. There was a tailed peak for gasification of wp-CNT as seen in the TPR profile of the Fe/wp-CNT catalyst

Table 3 shows reduction temperature for both catalysts. According to the reduction temperature, deposition of iron oxide particles inside the nanotubes with narrow pores results in a decrease in the temperature of the first TPR peak from 459 to 401°C and that of the second TPR peak from 574 to 438°C. The degree of reduction for the Fe/np-CNT and Fe/wp-CNT catalysts is also given in Table 3. The degree of reduction of the metal is the ratio of H_2 consumed from ambient temperature to 700°C to the calculated amount of H_2 for the complete reduction of metal oxides.

According to Table 3, the degree of reduction for Fe/np-CNT (69%) was higher than that of Fe/wp-CNT (52%). This can result in partial reduction of metal sites in the case of the Fe/wp-CNT catalyst and lower FT activity. According to the literature, in the case of FT catalysts with average particle size of larger 10 nm, the particle size does not affect the extent of reduction [4]. Thus, this phenomenon may be attributed to a different interaction of iron oxide with interior surface of the Fe/np-CNT catalyst compared to that of the Fe/wp-CNT catalysts. As reported by other researchers [7, 8], the confinement of iron oxide inside in the CNT pores results in easier reduction at lower temperature. It has been postulated that the electron deficiency of the interior CNT surface is possibly responsible for this phenomenon and extent of this phenomenon decreases as inner diameter of nanotube increases.

4 Fischer–Tropsch synthesis

The performances of the Fe/np-CNT and Fe/wp-CNT catalysts for the FT synthesis were evaluated in a fixed bed reactor. All the reactions were performed under a set of similar conditions (275°C, 2MPa, H_2:CO = 2). CO hydrogenation (blank runs with no iron) was performed on both acid treated CNT supports (np-CNT and wp-CNT samples) under the same operating conditions as the metal loaded samples. For blank runs, the main product formed with a very low conversion (1%) was methane with almost no higher hydrocarbons.

The activity and product selectivity (% CO conversion, CH_4, C_2-C_5, C_5+ and CO_2) of the catalysts is given in Table 4. According to Table 4, the Fe/np-CNT catalyst showed a CO conversion of 30.7% whereas; this number for the Fe/wp-CNT catalyst was only 12.2%. Also, CH_4 selectivity of the Fe/np-CNT

(14.7 wt%) catalyst was much lower than that of the Fe/wp-CNT catalyst (41.1wt%). Accordingly, C_5+ selectivity of the Fe/np-CNT (48.1 wt%) was considerably higher than that of Fe/wp-CNT (11.9 wt%).

Table 4: CO conversion and product selectivity of Fe/np-CNT and Fe/wp-CNT.

Catalyst activity and product selectivity	Fe/np-CNT	Fe/wp-CNT
CO%	30.7	12.2
CH_4	14.7	41.1
C_2-C_4	37.3	47.1
C_5+	48.1	11.9
CO_2	19.5	15.0

- Process conditions: 7.2 Nl/g-cat/h, 2MPa, $H_2/CO = 2$.
-All catalysts contain 20wt% Fe.
-HC in wt%; CO_2 in mol%.

The result of FT analysis for both Fe/np-CNT and Fe/wp-CNT catalysts showed that the deposition of iron particles inside the nanotube pores with narrower pores within the range of studied pore diameters (higher than 10 nm) enhances FT activity and product selectivity of the catalyst. Several reasons can be associated with the improvement in activity and product selectivity. As discussed earlier, H_2-TPR analysis revealed that the reducibility of the Fe/np-CNT catalyst was remarkably better in comparison to the Fe/wp-CNT. This phenomenon can result in the formation of more catalytically active carbide species during FTS. Also, confinement of the reaction intermediates inside the pores can enhance their contact with iron catalysts, favoring the growth of longer chain hydrocarbons.

As given in Table 4, CO_2 selectivity of the Fe/wp-CNT was less than that of the Fe/np-CNT catalyst. This can be resulted from lower CO conversion for the Fe/wp-CNT catalyst. At a low CO conversion, the amount of the produced water was lower which provided a lower water concentration for water-gas-shift reaction during the FT reactions.

5 Conclusions

The results of this work revealed that the structure and pore diameter of CNTs as support for FT catalysts have significant influence on the catalytic performance of the catalysts. The deposition of metal particles inside the nanotube with narrow pore structure resulted in smaller metal particle sizes and better dispersion due to confinement effects inside CNT pores. Also iron catalyst supported on the narrow pore support improved the reduction behavior of the CNT catalyst most likely due to difference in electronic properties of the inner surface of the CNTs with different diameters. Higher metal dispersion and better extent of reduction resulted in more active and selective catalysts. In the case of

catalysts with metal particles inside the narrow pores, confinement of reaction intermediates inside the channels may also increase the contact time with active metal sites, resulting in production of heavier hydrocarbons.

References

[1] Dry, M. E., Fischer–Tropsch reactions and the environment. *Applied Catalysis A: General* **189** pp. 185-190, 1999.
[2] van der Laan, G. P. & Beenackers, A. A. C. M., Kinetics and Selectivity of the Fischer–Tropsch Synthesis: A Literature Review. *Catalysis Reviews*, **41(3&4),** pp. 255-318, 1999.
[3] Bukur, D. B., Lang, X., Mukesh, D., Zimmerman, W. H., Rosyenek, P. & LI, C., Binder/Support Effects on the Activity and Selectivity of Iron Catalysts in the Fischer–Tropsch Synthesis, *Industrial Engineering Chemistry Research*. **29**, pp. 1588-1599, 1990.
[4] Khodakov, A. Y., Griboval-Constant, A., Bechara R. & Zholobenko, V. L., Pore Size Effects in Fischer Tropsch Synthesis over Cobalt-Supported Mesoporous Silicas, *Journal of Catalysis* **206**, pp. 230–241, 2002.
[5] Malek Abbaslou, R. M., Tavasoli, A. & Dalai, A. K., Effect of pre-treatment on physico-chemical properties and stability of carbon nanotubes supported iron Fischer–Tropsch catalysts, *Applied Catalysis A: General* **355**, pp. 33–41, 2009.
[6] Tavasoli A., Malek Abbaslou R. M., Trepanier M. & Dalai A. K., Fischer–Tropsch synthesis over cobalt catalyst supported on carbon nanotubes in a slurry reactor, *Applied Catalysis A: General* **345**, pp. 134–142, 2008.
[7] Chen, W., Pan, X. & Bao, X., Tuning of Redox Properties of Iron and Iron Oxides via Encapsulation within Carbon Nanotubes, *Journal of American Chemical Society*, **129**, pp. 7421-7426, 2007.
[8] Chen, W., Fan, Z,, Pan, X. & Bao, X., Effect of Confinement in Carbon Nanotubes on the Activity of Fischer–Tropsch Iron Catalyst, *Journal of American Chemical Society*, **130**, pp. 9414-94192008
[9] Bahome, M. C., Jewell, L. L., Hildebrandt, D., Glasser, D. & Coville, N. J., Fischer–Tropsch synthesis over iron catalysts supported on carbon nanotubes, *Applied Catalysis A: General* **287**, 60-67, 2005.
[10] Ma, W., Kugler, E. L., Wright, J. & Dadyburjor, D. B., Mo-Fe Catalysts Supported on Activated Carbon for Synthesis of Liquid Fuels by the Fischer–Tropsch Process: Effect of Mo Addition on Reducibility, Activity, and Hydrocarbon Selectivity , *Energy & Fuels* **20**, 2299-2307, 2006.
[11] Serp P., Corrias M. & Kalck P., Review Carbon nanotubes and nanofibers in catalysis, *Applied Catalysis A: General* 253, 337-358, 2003.
[12] Eswaramoorthi I., Sundaramurthy V.& Dalai A.K., Partial oxidation of methanol for hydrogen production over carbon nanotubes supported Cu-Zn catalysts, *Applied Catalysis A: General* **313,** pp. 22-28, 2006.